View metadata, citation and similar papers at core.ac.uk

brought to you by CORE

provided by Institutionelles Repositorium der Leibniz Universität Hannover

Research Article | Vol. 27, No. 26 / 23 December 2019 / Optics Express 38326

Optics EXPRESS

Experimental and theoretical study of the formation process of photopolymer based self-written waveguides

MONALI SUAR,[1,2,*] OLIVER MELCHERT,[1,2,3] MAIK RAHLVES,[1] AND BERNHARD ROTH[1,2]

[1]*Hannover Centre for Optical Technologies, Leibniz Universität Hannover, Nienburger Str. 17, 30167 Hanover, Germany*

[2]*Cluster of Excellence PhoenixD, Leibniz Universität Hannover, Welfengarten 1, 30167 Hannover, Germany*

[3]*Institute of Quantum Optics (IQO), Leibniz Universität Hannover,30167 Hannover, Germany*

[*]*monali.suar@hot.uni-hannover.de*

Abstract: The realization of optical interconnects between multimode (MM) optical fibers and waveguides based on a self-writing process in photopolymer media represents an efficient approach for fast and easy-to-implement connection of light-guiding elements. When light propagates through photopolymer media, it modulates the material properties of the media and confines the spreading of the light beam to create a waveguide along the beam propagation direction. This self-writing process can be realized with a single photopolymer medium and is also suited to connect optical fibers or waveguides with active elements such as light sources and detectors. Numerical simulations of the underlying light-induced polymerization process is carried out by using a diffusion based material model which takes account both monomer diffusion and its conversion to polymer chains in regions exposed to light fields. In this work experimental results obtained from a one-polymer approach are validated with theoretical predictions from the diffusion model. The study involved the demonstration of temporal dynamics and transmittance from self-written waveguide (SWW) couplers during the self-writing process. The measured attenuation coefficient from experiment $\alpha_{experiment} = (8.43 \pm 0.3) \times 10^{-5}$ dB/µm showed good agreement with the theoretically predicted attenuation coefficient $\alpha_{simulation} = 7.93 \times 10^{-5}$ dB/µm, thus demonstrating a successful application of the diffusion model to epoxy based acrylate SWWs. For comparison, attenuation measurements between optical fibers with SWWs as interconnects and one without SWW, i.e. with an air gap in between, were performed. The obtained results reveal that the theoretical approach correctly describes the waveguide formation process so that in the next step the studies can be extended towards including further relevant parameters such as temperature.

Published by The Optical Society under the terms of the Creative Commons Attribution 4.0 License. Further distribution of this work must maintain attribution to the author(s) and the published article's title, journal citation, and DOI.

1. Introduction

Polymer-based optical interconnects attracted much attention in recent years as they can be used in integrated photonic circuits of telecommunication networks. The main reason behind this is that these interconnects are lightweight, easy to process, highly flexible, and ultimately low-cost. Various approaches were proposed to fabricate these types of interconnects, e.g., hot embossing [1], femtosecond laser writing [2], photolithograpy [3,4] and direct laser ablation [5]. A very simple and reliable technique to fabricate optical interconnects exploits self-writing of the waveguides in polymer which was first proposed by Frisken [6]. The SWWs are created by the self-action of light where the excitation beam is focused and trapped within the material medium

#375049 https://doi.org/10.1364/OE.27.038326
Journal © 2019 Received 14 Aug 2019; revised 25 Sep 2019; accepted 3 Nov 2019; published 18 Dec 2019

Optics EXPRESS

due to self-induced change in the refractive index along the direction of beam propagation. This photopolymerization mechanism is local in space but non-local in time, i.e., the refractive index modulation is higher in large intensity areas and also depends on the history of the electromagnetic fields at earlier times, very much similar to the Kerr effect. In contrast to the latter, this mechanism provides the possibility to write SWWs with low intensity laser beams [7]. Some other advantages of SWWs include rapid response time (in seconds) compared to photosensitive glass (in hours) during fabrication, high sensitivity relative to low exposure intensity and permanent structure formation under suitable conditions [8]. The SWWs are also called self-induced waveguides as they are fabricated by propagating a light beam through photopolymer media and they can guide beams of different polarization or wavelength. This process provides a very relaxed alignment technique between the light source and the propagating media employed for the SWWs. They can be used as interconnects between different optical components (fiber-to-fiber, laser-to-fiber, laser-to-laser and optical sensors) in integrated photonic circuits or in polymer back-planes. Many theoretical and experimental studies were already carried out to understand the underlying self-writing phenomenon of the light within photo-monomer as well as in other photosensitive materials [9–17].

In this Letter, experimental as well as theoretical studies of polymer based SWWs with respect to the evolution of intensity profiles of SWWs and their transmittance during the writing mechanism are reported. The intermediate SWW coupling structures between two multimode fibers are used as illustrative examples because of the simple fabrication process. The attenuation was calculated for polymer based SWWs and then compared with the structures without SWW, i.e. with an air gap.

The one-polymer approach to create solid SWWs is described in our earlier work [18]. Compared to a two-polymer approach to realize the core and cladding of the interconnect structure, this approach is simpler and does not require the removal of the residual core material after the self-writing process [19]. Also, in this work, we use one single writing wavelength to realize both core and cladding whereas in the two polymer approach two writing wavelengths have to pass through the photo-monomer sample to induce different refractive index modulations in the core and cladding region of the SWW, respectively. This is due to the fact that the polymers exhibit different sensitivities in different wavelength regions. The one polymer approach was first introduced by Missine *et al.* [20] for commercially available Norland optical adhesive NOA68 and further modified by Günther *et al.* [21] by applying the approach to a novel polymer, i.e. SynIII. The photopolymer liquid used in our experiment was a mixture of two compounds: an epoxy based acrylate, Syntholux 291 EA (93 wt.%), from Synthopol (Buxtehude, Germany) which is UV-curable with 80 wt.% TPGDA (tripropylene glycol dimethaacrylat), and 2,3-butanedione (7 wt.%) from Sigma-Aldrich (Taufkirchen, Germany) also known as biacetyl which acted as the photo-initiator. To prepare the photopolymer mixture, 30 g of Syntholux and 2.2 g of Biacetyl were measured using an electronic weighing scale. These two starting materials were mixed for 3 hours by the use of a hand mixture to obtain homogeneity under standard room conditions. The resulting transparent mixture was kept overnight within a vacuum chamber in a dark room to remove air bubbles. Then the self-written waveguides are created within the prepared photopolymer liquid.

2. Simulation model

The simulation approach for SWWs relies on applying the paraxial approximation to the Helmholtz equation to yield the beam propagation equation, Eq. (1).

$$2in_0k_0\frac{\partial u(x,z)}{\partial z} = \frac{\partial^2 u(x,z)}{\partial^2 x} + k_0^2(n(x,z)^2 - n_0^2)u(x,z). \tag{1}$$

Optics EXPRESS

Therein, $n(x, z)$ is the refractive index and n_0 is the average value of the refractive index, k_0 is the free space wave number and $u(x, z)$ is the electric field envelope amplitude of the electromagnetic waves. The transverse and propagation directions are denoted by x and z, respectively. We use a Crank-Nicholson (CN) based finite difference scheme in conjunction with transparent boundary conditions (TBCs) to solve Eq. (1) and to accurately describe the beam intensity profiles of the optical coupler [22]. The two-dimensional (2D) beam propagation method (BPM) scheme is coupled to a diffusion material model to obtain the induced change in the refractive index of the medium upon propagation of laser light along the propagation direction z. In this process, the temporal modulation of the refractive index is a complex phenomenon which accounts for the redistribution of the individual components during the simulation and requires the solution of the partial differential equations:

$$\frac{\partial M(x,z,t)}{\partial t} = \nabla(D\nabla M(x,z,t) - K_r M(x,z,t) I(x,z,t)\Big(1 - \frac{\triangle n(x,z,t)}{\triangle n_f}\Big), \tag{2}$$

$$\frac{\partial P(x,z,t)}{\partial t} = K_r M(x,z,t) I(x,z,t)\Big(1 - \frac{\triangle n(x,z,t)}{\triangle n_f}\Big). \tag{3}$$

Here, M and P are the concentrations of monomer and polymer, respectively. The diffusion constant and polymerization rates are denoted by D and K_r. The first part of Eq. (2) describes the diffusion of the monomer from the region not illuminated by light to the neighboring bright region and the second part marks the simultaneous conversion of the monomer to long polymer chains. The polymer chains are too heavy to move, so the diffusion coefficient is neglected for polymer evolution and its redistribution is governed by Eq. (3). The saturation in refractive index is achieved by the term $\Big(1 - \frac{\triangle n(x,z,t)}{\triangle n_f}\Big)$, where the maximum attainable refractive index value is $\triangle n_f$ and $\triangle n(x, z, t)$ is the refractive index difference between the core and cladding part of the SWW. The 2D Laplace operator $\triangle$ is given by $\nabla^2 = \frac{\partial^2}{\partial x^2} + \frac{\partial^2}{\partial z^2}$ and $I(x, z, t)$ is the light intensity. The evolution of the refractive index of the material at any particular time t is calculated via the Lorentz-Lorenz relation [23],

$$\frac{n^2 - 1}{n^2 + 2} = \Phi_m \frac{n_m^2 - 1}{n_m^2 + 2} + \Phi_p \frac{n_p^2 - 1}{n_p^2 + 2} + \Phi_a \frac{n_a^2 - 1}{n_a^2 + 2}, \tag{4}$$

where the volume fractions of monomer, polymer, and photo-initiator are expressed by Φ_m, Φ_p, and Φ_a, respectively. n_m, n_p and n_a are their corresponding refractive indices. By knowing the concentrations, densities and refractive indices of the individual components, their respective volume fractions are calculated by taking into account the conservation principle of total volume fraction, i.e., $\Phi_a + \Phi_m + \Phi_p = 1$. Details of the calculation process follow from the work of Babeva *et al.* [24]. A series of numerical investigations carried out on SWWs by using a diffusion based material model are well described in [25]. The diffusion constant $D = 6 \times 10^{-15}$ m^2/s is considered for the simulation and measured experimentally in [26]. It is possible to set different values for the rate constant K_r which affects the curing time of the SWWs. In this work, K_r was fixed at 0.005 as all simulations run for a total time of 10 min. The refractive index value for monomer n_m, polymer n_p, and photo-initiator n_a, are extracted from product data sheets and fixed at 1.52, 1.55 and 1.39 respectively. The simulation started with initial conditions of 93% monomer and 7% photo-initiator which are the same as the one prepared for the experiment. A

Optics EXPRESS

Gaussian beam is used as excitation source with initial distribution

$$u(x, z = 0) = \exp\left(-\frac{x^2}{x_0^2}\right). \tag{5}$$

Here, x_0 is the half width of the input laser beam. The step increments were chosen as $\Delta x = 0.5\,\mu$m, $\Delta z = 1\,\mu$m, and $\Delta t = 1$s for the convergence of the finite difference scheme. The simulation proceeded in a temporal loop. The induced change in refractive index is calculated by the material model which is then passed to the CN-BPM algorithm to compute the new light intensity distribution for each time iteration. Günther *et al.* have earlier demonstrated the multimode Gaussian shape of the refractive index profile for these SWW interconnects in the photopolymer sample (see the fourth figure in [21]). So, for simplicity, we considered a Gaussian beam formula to obtain the numerical results.

3. Experimental setup

The experimental schematic for the fabrication of optical interconnects between two opposing multi-mode (MM) fibers is shown in Fig. 1. Laser illumination at 638 nm from a 4-channel laser source (Thoslabs MCLS1, Germany) is further passed through 50/50 beam splitter (TW630R5F1, ThorLabs), dividing the incoming beam into two equal halves which is then fed into MM fibers of different core diameters. M42L05-FG050LGA (ThorLabs) and M43L05-FG105LCA (ThorLabs) were used as the incoming and outgoing MM fibers. The MM fibers are aligned with each other by the help of a manual positioning stage which provided five alignment axes along lateral and axial directions. The precise positioning of the waveguiding structures, i.e. optical fibers in this case, was crucial as the fabrication of SWWs occurs only in the overlap region of the two light beams. An external white LED lamp (SCHOTT, VisiLED ring S80-55) fixed on the top of the setup is used to trigger and control the polymerization process. A microscope objective and a CCD camera which was connected to a personal computer are carefully placed over the fibers to capture images during the curing process. The MM fiber ends were inserted into the photo-monomer liquid mixture using the 5-axes positioning stage. When physical connection was established between the opposing fibers, the right side collecting fiber (CF) was detached from the beam-splitter and coupled to the power detector, PD (S120C, ThorLab, Germany) to monitor the transmitted intensity continuously. It is also possible to completely eliminate the 50/50 beam splitter from the experimental set-up, i.e., a single incident laser beam is then launched to the

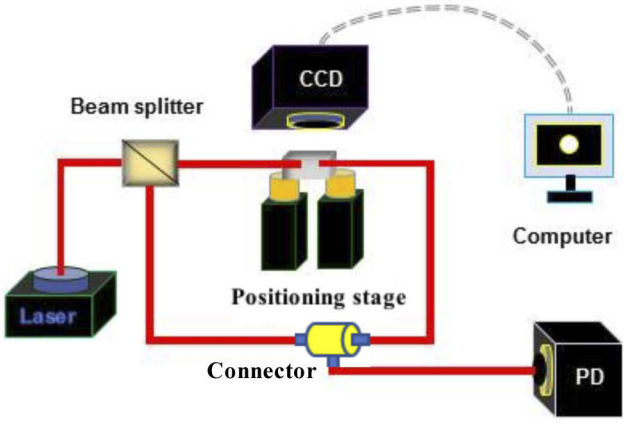

Fig. 1. The schematic of the experimental set-up for fabrication of SWWs. CCD : Charged Coupled Device, PD : Power Detector.

Optics EXPRESS

MM fiber on the left side, then propagates through the photo-monomer mixture, and finally the transmitted power is recorded from the collector MM fiber on the right side. This approach is called one-way writing and requires precise alignment of the fiber ends. Here, the light beam between the MM fibers was adjusted by using the positioning stage. It was easy to couple the laser beam from the incoming MM fiber which had a beam diameter of 50 µm into the collecting MM fiber which had a larger beam diameter of 105 µm. Also, the writing-lengths were kept small between 0 to 1000 µm for the fabricated SWWs. The numerical aperture NA was 0.22 for both these MM fibers. We also performed writing with two beams, called two-way writing, to create SWWs and found no dependence of the attenuation on writing direction as the writing power and wavelength are kept in the same range for all experiments. The BS was only used for the two-way writing process and was omitted for the one-way writing process. Both one-way and two-way self-writing were performed initially to investigate the correlation between attenuation and the writing directions. Afterwards, only the one-way approach was followed for all experimental results provided in this work, as we observed no dependency between attenuation and writing directions. The second arm in the setup in Fig. 1 does not provide any advantage for the one-way writing approach for straight SWWs, thus. After launching the laser beam, the initial trajectory of the beam was observed between the MM fibers. However, the SWWs were not fully evolved at this stage and the trajectories can be bent with any change in the position of the input beam. To create all solid polymer waveguide and interconnects, application of an external excitation source (white light LED) is required to cure the core and cladding. In our case, the writing was carried out for 10 min for most SWWs, although a stabilized output power was observed after 4 min.

The photopolymer media supported the writing of the SWWs at both 406 nm and 638 nm. The transmission spectra for the uncured and cured photopolymer media can be found in the earlier work of our group in Fig. 2 of [21], where a steep absorption edge was observed between 360 nm and 480 nm. The preferred writing wavelengths can be considered in the range of 480 nm

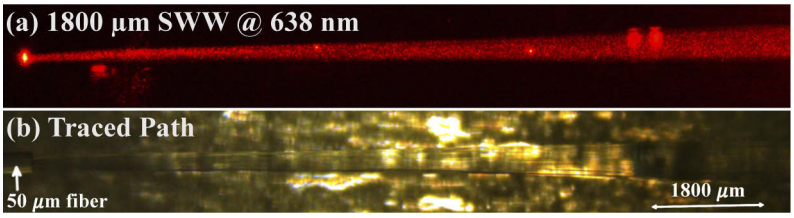

Fig. 2. (a) An SWW with a length 1800 µm is created by a laser beam at 638 nm with 15 mW power from a MM fiber having a 50 µm core diameter, (b) the traced path remained in the sample after removal of excitation. The light propagates from left to right.

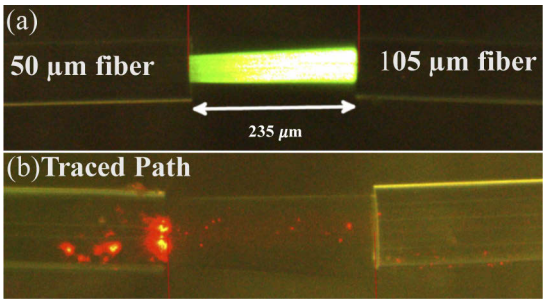

Fig. 3. (a) A 235 µm SWW created between MM fibers (different diameters) at a wavelength of 406 nm and a power of 800 µW. (b) A beam at 638 nm propagates in the existing channel. The light propagates from left to right.

Optics EXPRESS

to 900 nm. In one example, an SWW of 1800 µm length was created by using a laser source at 638 nm having a power of 15 mW and launched from a MM fiber of 50 µm core diameter, see Fig. 2(a). The inscribed path of the light remained within the sample after writing was completed, marked as the traced path in Fig. 2(b). Another SWW with a length of 235 µm was created between two MM fibers by using a 406 nm laser beam having a power of 800 µW, as shown in Fig. 3(a). The diameters of incoming and collecting fibers were 50 µm and 105 µm, respectively. A larger core diameter collecting MM fiber was used for easy beam coupling. In case of same core diameters of both fibers, one could use an objective lens after the incoming fiber to focus the beam into the other end. It is also possible to propagate a wavelength other than the writing wavelength within the SWW after its fabrication. One such example is demonstrated in Fig. 3(b). The captured images are at different magnification scales of the microscopic camera. The refractive index difference between the core and the cladding of the SWW at a writing wavelength 638 nm was $\Delta n = 4 \times 10^{-4}$ as reported by our earlier study in [18]. Most prepared SWWs had a diameter of 100 µm and so they supported 49 propagating modes.

4. Results and discussion

The temporal dynamics of a SWW during the writing process from experiment and simulation are illustrated in Fig. 4 and Fig. 5, respectively. The photosensitive medium described in the Introduction section is also used here to obtain the below experimental results. A laser source at 638 nm with 15 mW power is used for writing of the SWW as it provided about 90% transmission efficiency minimizing the absorption for the photopolymer sample at this writing wavelength, see [21]. In the experiment, the images were captured during the initiation of the laser excitation, after 1 min, and after 3 min, respectively, as shown in Fig. 4. Here, the interconnect was written between the input MM fiber with a 50 µm core diameter and an output MM fiber with a 105 µm core diameter. The core diameter of the collecting MM fiber was larger than the incoming MM fiber for easy alignment and beam guiding purposes. Light scattering is observed as red dots before commencement of material modulation as seen in Fig. 4(a). Just after 1 min, the spreading of light beam is narrower and confined to a fine thin line, see Fig. 4(b), where the refractive index of the medium is increased from the initial value. However, the confinement of the beam is not yet sufficient. After 3 min, sufficient material modulation is induced resulting in the creation of an SWW with complete beam guidance, as seen in Fig. 4(c). The simulation was carried out for a straight SWW by propagating a Gaussian beam through the material and observing the evolution of the temporal dynamics of the intensity profiles, see Fig. 5. We observed a very similar evolution pattern for the SWW in the simulation compared to the experiment. Initially, the beam was spreading prominently in the computational image, in Fig. 5(a). It was then decreased at a later time at 17 s due to increase in refractive index along the direction of the beam propagation axis, see Fig. 5(b). Here, the maximum focus point of intensity was created near to the excitation port which afterwards started to move along the optical axis of the SWW, see Fig. 5(c). This indicates a signature of good light guiding of the SWW depicting the attainment of sufficient refractive index modulation for beam confinement [9,27,28]. The evolution mechanism of an SWW from experiment agrees well with the evolution of intensity profiles of the SWW from simulation. The spatial beam dispersion to surrounding media is observed in both Fig. 4(a) and Fig. 5(a). After some time, the refractive index along the beam propagation direction increased leading to the self-focusing of the light beams, see Fig. 4(b) and Fig. 5(b). The dispersion is reduced as the liquid is modified in experiment. The primary eye formed near to the excitation input port in the simulation which shows the self-focusing effect of the beam as the SWW is just formed within the medium. However, the SWWs are not stable and fully evolved at this stage. The induced change in refractive index continues to increase and after some time instances, the light beams are completely self-trapped to create stable and evolved SWWs, see Fig. 4(c) and Fig. 5(c). The transmitted intensity stabilizes at a maximum for the SWW in experiment in Fig.

Optics EXPRESS

4(c). In the simulation, we have observed the movement of the primary eyes as the light beam is complete guided within the SWW in Fig. 5(c).

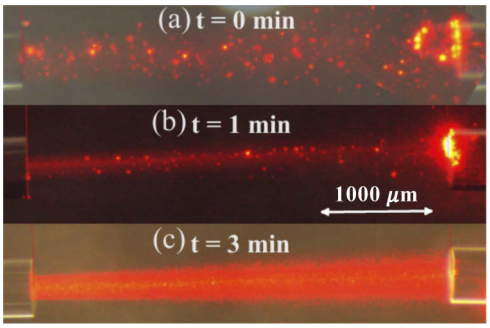

Fig. 4. Evolution of a straight waveguide in experiment. The light propagates from left to right.

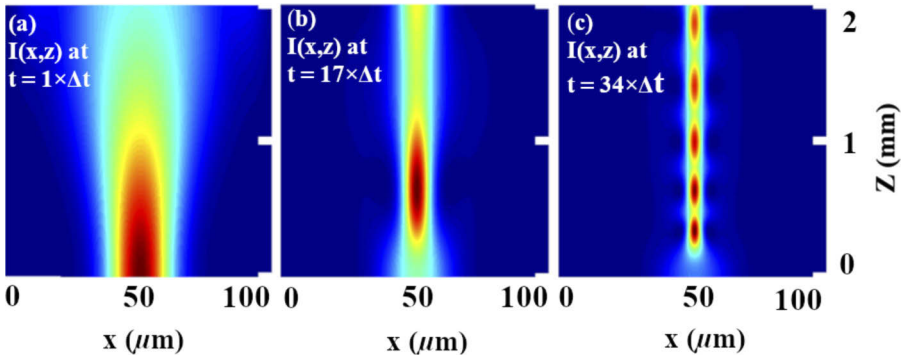

Fig. 5. Intensity profile I(x,z) as function of time t demonstrating the formation of a straight SWW during an exemplary simulation. (a) Intensity profile at time $t = \Delta t$, (b) at $t = 17\Delta t$, and (c) at $t = 34\Delta t$. $\Delta t = 1$ s (the time increment step size). For details, see text.

The transmitted intensity from the output port of a 340 µm long SWW is recorded continuously for 10 min during the writing process in the experiment and also in simulation. Here, the one-way writing approach is used to record the transmission from the SWWs in experiment. A laser beam at a wavelength of 638 nm is coupled to a 50 µm fiber to write the SWW. Figure 6(a) shows the variation of the transmitted power recorded by the power detector (PD) which was coupled to the output port of the collector fiber. Initially, the output intensity remained at 1 mW when only the laser excitation is provided. Then, the external white LED is switched on in addition to the laser. The LED can be controlled in a range of 1 to 8 where the maximum corresponds to an illumination of nearly 200 klx. The illumination from the LED was gradually increased till $t = 100s$ and afterwards kept at the maximum. One can control the curing time by regulating the intensity illumination of the LED. We observed a steady increase in transmitted power till the maximum intensity value of 5.1 mW was reached after 100 s. It remained at this intensity value until $t = 200s$ and then a decrease in intensity is observed which is followed by another rise and stabilization phase. The dip in the transmitted intensity could be due to a different modulation of the refractive indices of the core and cladding region, i.e. possibly at this point, the refractive index of the outer cladding part of the sample is increasing faster compared to the inside core area as the former starts to solidify. A dip was observed in the transmission intensity for few seconds before it recovered and stabilized. At this point, we assume that the refractive

Optics EXPRESS

index difference (△n) between core and cladding of the SWW decreased from the previous time instant, however n_{core} was always higher than $n_{cladding}$ during the whole curing process. So, the difference in refractive index between the core and the cladding is reduced which has a direct impact on the power the waveguide is carrying. When the transition stage is crossed and the sample completely changed to fully solid, the transmitted intensity saturates. The transmittance in Fig. 6(a) is of qualitative nature. In future, we will carry out a quantitative study to yield more accurate transmittance values. The transmitted power can also be calculated from the material model in the simulation of the temporal evolution of the SWW. Here, the transmitted power increased steadily and smoothly from zero towards the maximum value and becomes stable when the liquid sample is completely polymerized, as shown in Fig. 6(b). This situation reflects the ideal case and additionally does not consider the illumination with the white light LED.

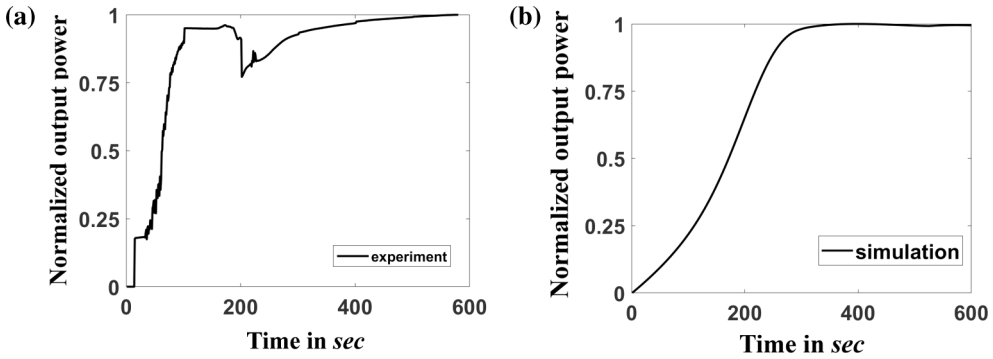

Fig. 6. Transmitted power during the writing process. (a) Normalized transmitted power as recorded by the power detector for a 340 µm long SWW in experiment. (b) Normalized output power for a 340 µm long SWW in the simulation.

Furthermore, attenuation measurements for interconnects ranging from 0 to 1000 µm length are performed at a wavelength of 638 nm. The laser beam is coupled to the input fiber with a core diameter of 50 µm and the transmitted power is received at the collecting fiber having core diameter of 105 µm. SWWs of 115 µm, 230 µm, 460 µm, 575 µm, 690 µm, 805 µm, and 920 µm lengths were realized between these MM fibers. The experimental measurements were repeated four times at each length scale of the SWW to obtain better accuracy for the measured losses. We again followed the fabrication process detailed in [21]. In the first step, opposing MM fiber ends were butt coupled without residual gap. Then, a liquid drop of photo-monomer resin mixture was placed over the fiber tips and the measured maximum transmitted intensity I_0 was noted. In the second step, the fiber positions were separated to create the above-mentioned gap length l in between them. Then, the laser was launched from the incoming fiber towards the collecting fiber and the SWW was cured while keeping the external LED on. The losses $L_{dB}(l)$ for SWWs were calculated by using

$$L_{dB}(l) = 10 * \log(I_0/I_l). \tag{6}$$

Here, the transmitted power I_l is measured after the writing was completed. I_l is normalized to the transmitted power of the butt-coupled case I_0, for attenuation calculations. So, the fiber based effects including the Fresnel reflections were subtracted from the actual measurement as we assumed a 0 dB loss at an interconnect length of 0 µm.

All calculated losses from the experimental measurements as given as red dots in Fig. 7. A linear fit was applied to these data points and the gradient of the linear fit yields the attenuation coefficient $\alpha_{experiment} = (8.43 \pm 0.3) \times 10^{-5}$ dB/µm at 638 nm as shown in Fig. 7. The standard deviation (SD) is also computed for each data set and length (l) and the mean value determined, see green circles, in Fig. 7. The size of the error bars increased as the length of the SWWs

Optics EXPRESS

increased. To validate the obtained experimental results, SWWs between 0 and 1000 µm in steps of 50 µm were simulated by using the diffusion based material model. The mode field radius x_0 of the Gaussian laser beam in the simulation is kept at 25 µm which is half the core diameter of the input MM fiber in the experiment at a writing wavelength of 638 nm. The refractive index modulation between the core and cladding of the SWW for the resin mixture consisting of Syntholux as the monomer and biacetyl as the photoinitiator was found to be $\Delta n = 4 \times 10^{-4}$ [18]. So, the evolving SWW was extracted from the diffusion material model for this refractive index modulation between core and cladding. The losses were calculated for the simulated SWW and the procedure was repeated for all length scales. Here, a linear fit yields the attenuation coefficient $\alpha_{simulation} = 7.93 \times 10^{-5}$ dB/µm. The losses from the simulation closely follow the experimental data, as shown in Fig. 7, and the linear fit to the simulation results was within the range of uncertainty specified from the experiment. Also, the attenuation was measured for air-gaps of same length between the MM fibers. The core diameters of fibers are as before. The losses were again calculated using Eq. 6, where I_0 is the input power, I_l is the transmitted power when the air-gap length was l, i.e., without any photo-monomer resin applied on the fiber tips. The calculated losses are shown as points in Fig. 8. A linear fit applied to them provides the attenuation coefficient $\alpha_{air} = 10^{-3}$dB/µm which is 11 times higher than for the polymer-based SWW. Here, all loss measurements were normalized to the maximum butt-coupled transmitted power and a linear fit was applied to the attenuation measurements, in Fig. 7 and Fig. 8, respectively. The attenuation coefficient for SWWs from experiment was $\alpha_{experiment} = (8.43 \pm 0.3) \times 10^{-5}$ dB/µm, see Fig. 7, and the one for the air gap case was $\alpha_{air} = 10^{-3}$dB/µm, see Fig. 8, at 638 nm. This shows that the SWWs are much more efficient interconnects compared to the air-gap (no SWW) case.

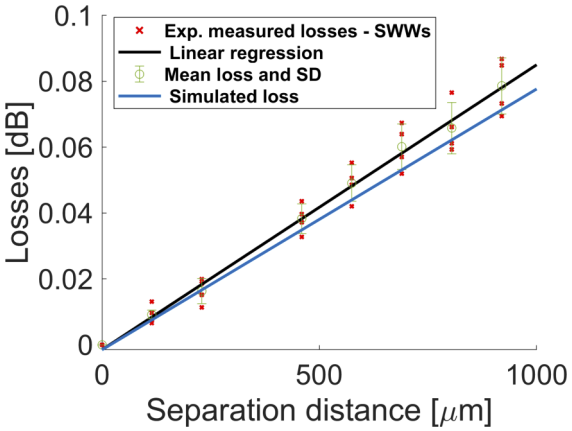

Fig. 7. Loss measurements at 638 nm for polymer SWWs from experiment and simulation.

Optics EXPRESS

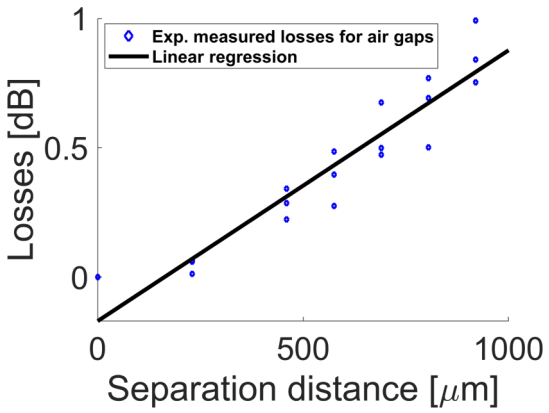

Fig. 8. Loss measurements at 638 nm for the case of an air gap between the fibers in experiment.

5. Conclusion

In summary, we performed a combined experimental and theoretical study to investigate the effects relevant for the self-writing of optical interconnects inside a single monomer resin. Self-focusing and self-trapping of the light is observed during the writing process of SWWs in the experiment and also in simulation. We recorded the transmitted output power from manufactured SWWs for 10 min in experiment, i.e., during the writing process which was then compared to the obtained transmitted power in simulation of the same SWW using a diffusion material model. Optical interconnects with length between 0 to 1000 µm were fabricated and their transmission losses measured in experiment. We find an attenuation coefficient $\alpha_{experiment} = (8.43 \pm 0.3) \times 10^{-5}$ dB/µm which is in good agreement with the predicted attenuation coefficient of $\alpha_{simulation} = 7.93 \times 10^{-5}$ dB/µm. Also, for the case of an air gap between the MM fibers, the losses were calculated and measured. The measured attenuation coefficient α_{air} was at 10^{-3} dB/µm was found to be 11 times higher than the attenuation of the SWWs. Our experimentally validated model of the writing process enables us to study the fabrication of optimized SWW interconnects in the future and is crucial for achieving high performance interconnects. Also, the influence of quantities such as temperature or stress on the SWW performance could be studied. .

Funding

Deutsche Forschungsgemeinschaft (EXC 2122, projectID 390833453); Gottfried Wilhelm Leibniz Universität Hannover.

Acknowledgments

We acknowledge support from the Deutsche Forschungsgemeinschaft (DFG) under Germany's Excellence Strategy within the Cluster of Excellence PhoenixD (Photonics, Optics, and Engineering Innovation Across Disciplines), (EXC 2122, projectID 390833453).

Disclosures

The authors declare no conflicts of interest.

References

1. M. Rezem, A. Günther, M. Rahlves, B. Roth, and E. Reithmeier, "Fabrication and sensing applications of multilayer polymer optical waveguides," Procedia Technol. **26**, 517–523 (2016).
2. W. M. Pätzold, C. Reinhardt, A. Demircan, and U. Morgner, "Cascaded-focus laser writing of low-loss waveguides in polymers," Opt. Lett. **41**(6), 1269–1272 (2016).

Optics EXPRESS

3. K. Tung, W. Wong, and E. Pun, "Polymeric optical waveguides using direct ultraviolet photolithography process," Appl. Phys. **80**(3), 621–626 (2005).
4. H. D. Nguyen, U. Hollenbach, U. Ostrzinski, K. Pfeiffer, S. Hengsbach, and J. Mohr, "Freeform three-dimensional embedded polymer waveguides enabled by external-diffusion assisted two-photon lithography," Appl. Opt. **55**(8), 1906–1912 (2016).
5. S. Zakariyah, P. Conway, D. Hutt, D. Selviah, K. Wang, J. Rygate, J. Calver, and W. Kandulski, "Fabrication of polymer waveguides by laser ablation using a 355nm wavelength Nd:YAG laser," J. Lightwave Technol. **29**(23), 3566–3576 (2011).
6. S. Frisken, "Light-induced optical waveguide uptapers," Opt. Lett. **18**(13), 1035–1037 (1993).
7. A. Kewitsch and A. Yariv, "Self-focusing and self-trapping of optical beams upon photopolymerization," Opt. Lett. **21**(1), 24–26 (1996).
8. H. Li, Y. Qi, J. P. Ryle, and J. T. Sheridan, "Self-written waveguides in a dry acrylamide/polyvinyl alcohol photopolymer material," Appl. Opt. **53**(34), 8086–8094 (2014).
9. T. M. Monro, L. Poladian, and C. M. de Sterke, "Analysis of self-written waveguides in photopolymers and photosensitive materials," Phys. Rev. E **57**(1), 1104–1113 (1998).
10. H. Li, Y. Dong, P. Xu, Y. Qi, C. Guo, and J. Sheridan, "Beam self-cleanup by use of self-written waveguide generated by photopolymerization," Opt. Lett. **40**(13), 2981–2984 (2015).
11. T. Yoshimura, D. Takeda, T. Sato, Y. Kinugasa, and H. Nawata, "Polymer waveguides self-organized by two-photon photochemistry for self-aligned optical couplings with wide misalignment tolerances," Opt. Commun. **362**, 81–86 (2016).
12. K. Dorkenoo, O. Crégut, L. Mager, F. Gillot, C. Carre, and A. Fort, "Quasi-solitonic behavior of self-written waveguides created by photopolymerization," Opt. Lett. **27**(20), 1782–1784 (2002).
13. A. Sukhorukov, S. Shoji, and Y. S. Kivshar, "Self-written waveguides in photosensitive materials," J. Nonlinear Opt. Phys. Mater. **11**(04), 391–407 (2002).
14. K. D. Dorkenoo, F. Gillot, O. Cregut, Y. Sonnefraud, A. Fort, and H. Leblond, "Control of the Refractive Index in Photopolymerizable Materials for (2 + 1) D Solitary Wave Guide Formation," Phys. Rev. Lett. **93**(14), 143905 (2004).
15. R. Malallah, D. Cassidy, I. Muniraj, J. P. Ryle, J. J. Healy, and J. T. Sheridan, "Self-written waveguides in photopolymer," Appl. Opt. **57**(22), E80–E88 (2018).
16. R. Malallah, H. Li, D. P. Kelly, J. J. Healy, and J. T. Sheridan, "A review of hologram storage and self-Written waveguides formation in photopolymer media," Polymers (Basel, Switz.) **9**(12), 337 (2017).
17. H. Li, Y. Qi, R. Malallah, and J. T. Sheridan, "Modeling the nonlinear photoabsorptive behavior during self-written waveguide formation in a photopolymer," J. Opt. Soc. Am. B **32**(5), 912–922 (2015).
18. A. Günther, S. Schneider, M. Rezem, Y. Wang, U. Gleissner, T. Hanemann, L. Overmeyer, E. Reithmeier, M. Rahlves, and B. Roth, "Automated misalignment compensating interconnects based on self-written waveguides," J. Lightwave Technol. **35**(13), 2678–2684 (2017).
19. M. Kagami, T. Yamashita, M. Yonemura, and A. Kawasaki, "Light-Induced self-written optical waveguides," IEICE Trans. Electron. **E90-C**(5), 1061–1070 (2007).
20. J. Missinne, S. Beri, M. Dash, S. Samal, P. Dubruel, J. Watté, and G. Van Steenberge, "Curing kinetics of step-index and graded-index single mode polymer self-written waveguides," Opt. Mater. Express **4**(7), 1324–1335 (2014).
21. A. Günther, A. Petermann, U. Gleissner, T. Hanemann, E. Reithmeier, M. Rahlves, M. Meinhardt-Wollweber, U. Morgner, and B. Roth, "Cladded self-written multimode step-index waveguides using a one-polymer approach," Opt. Lett. **40**(8), 1830–1833 (2015).
22. Lifante Pedrola Ginés, *Beam Propagation Method for Design of Optical Waveguide Devices* (John Wiley & Sons, 2015).
23. W. Heller, "Remarks on refractive index mixture rules," J. Phys. Chem. **69**(4), 1123–1129 (1965).
24. T. Babeva, I. Naydenova, D. Mackey, S. Martin, and V. Toal, "Two-way diffusion model for short-exposure holographic grating formation in acrylamide-based photopolymer," J. Opt. Soc. Am. B **27**(2), 197–203 (2010).
25. M. Suar, M. Rahlves, E. Reithmeier, and B. Roth, "Numerical investigations on polymer-based bent couplers," J. Opt. Soc. Am. B **35**(8), 1896–1904 (2018).
26. S. Gallego, A. Márquez, M. Ortu no, J. Francés, S. Marini, A. Beléndez, and I. Pascual, "Surface relief model for photopolymers without cover plating," Opt. Express **19**(11), 10896–10906 (2011).
27. O. Kashin, E. Tolstik, V. Matusevich, and R. Kowarschik, "Numerical investigation of the (1+1)D self-trapping of laser beams in polymeric films based on polymethylmethacrylate and phenanthrenequinone," J. Opt. Soc. Am. B **26**(11), 2152–2156 (2009).
28. R. Malallah, H. Li, I. Muniraj, D. Cassidy, N. Al-Attar, J. J. Healy, and J. T. Sheridan, "Controlling the trajectories of self-written waveguides in photopolymer," J. Opt. Soc. Am. B **35**(8), 2046–2056 (2018).

194.95.157.39 {ts '2021-02-17 07:11:26'}